Express Polymer Letters Vol.16, No.5 (2022) 488–499
Available online at www.expresspolymlett.com
https://doi.org/10.3144/expresspolymlett.2022.37

Research article

Network-level analysis of damage in amine-crosslinked diglycidyl ether resins degraded by acid

Jonathon Tanks[1*], *Yoshihiko Arao*[2], *Masatoshi Kubouchi*[3]

[1]National Institute for Materials Science, Research Center for Structural Materials, Tsukuba, Japan
[2]Waseda University, Department of Applied Mechanics and Aerospace Engineering, Tokyo, Japan
[3]Tokyo Institute of Technology, Department of Chemical Science and Engineering, Tokyo, Japan

Received 15 October 2021; accepted in revised form 5 January 2022

Abstract. Amine-crosslinked epoxy resins represent a large fraction of polymers used in structural and coating applications, meaning the characterization and modeling of environmental durability and mechanical reliability is of utmost importance. In particular, chemical storage tanks, sewage systems, and oil/gas infrastructure involve prolonged exposure to organic and inorganic acids. However, the majority of meso-scale models for polymer network degradation are more appropriate for hydrogels than stiff thermosets; meanwhile, other models developed for acid degradation of ester-containing networks are not applicable to amine-cured epoxies due to the assumption that crosslink density decreases. In this paper, we report the acid uptake and subsequent degradation behavior of bisphenol-F epoxy cured with an aliphatic amine, as well as propose a simple but physically meaningful model for an ideal 2D network that effectively relates acid uptake and polymer structure to the decrease in elastic properties over time. Parameters include crosslink density and acid penetration rate, and the only best-fit parameter is the reaction rate constant. This analysis can be extended to more complex network structures and environmental conditions to model neat resins and composites.

Keywords: *thermosetting resins, damage mechanism, mechanical properties, modelling and simulation*

1. Introduction

Epoxy represents one of the most commonly used thermosetting polymers for a variety of applications, including adhesives, anti-corrosion coatings, and composites. When used in acidic environments such as chemical storage tanks or sewer systems, the acid penetration rate and consequent degradation reactions must be characterized to inform lifetime predictions [1–7]. Anhydride-cured epoxy contains hydrolyzable ester groups, which means prolonged exposure to aqueous environments will lead to a decrease in crosslink density and subsequently mechanical properties [1, 3, 8–10]. These systems are rather convenient for evaluating such degradation behavior experimentally or analytically, since various techniques can be readily applied for measuring crosslink density, segmental molecular weight of leached reaction products, and relative concentrations of carbonyls [9, 10]. Amine-cured epoxy resins offer advantages over other types, such as low curing temperatures and high alkali resistance, but several studies have shown that their lifetime is reduced in acidic environments [1–4, 7, 11–14]. Nitric acid [15–17] and glacial acetic acid [18] have proven effective for breaking down the amine-epoxy network in the case of chemical recycling, but these acids are special cases compared to common inorganic acids such as H_2SO_4 and HCl. The relationship between specific degradation mechanisms and corresponding changes in mechanical properties that occur in amine-crosslinked epoxies have not been elucidated theoretically, despite numerous experimental observations [1–4, 18].

*Corresponding author, e-mail: tanks.jonathon@nims.go.jp

Tanks *et al*. [19] proposed a degradation model that elucidates the relationship between network structure and equilibrium acid uptake through an aryl ether cleavage-based chain scission scheme, namely: (1) dehydration of hydroxyls near crosslink sites to form enol-ether intermediates, followed by (2) hydration of the protonated intermediate to form an aldehyde and phenol. This pathway can be found in biodegradation studies on compounds containing aryl ether linkages [20, 21]. However, in order to apply such a degradation model to the life prediction of epoxy resins (*i.e.*, prediction of long-term mechanical properties), another model is necessary for connecting the molecular scale and the bulk scale – a so-called meso-scale 'black box' model.

Shaw [22] conducted a chain-level analysis of untangled elastomers to show how random scission due to oxidation or mechanical load decreases long-term stiffness. This is a purely physical model that relates elastic properties to the network connectivity, without consideration for time-dependent processes or molecular structure of the network. Several other key studies [23–30] have proposed network-level analytical models for polymer degradation, but they are specifically intended for hydrogels and consider mass-loss/molecular weight as the target variable for predicting degradation. Furthermore, these models apply to polymers with reactive crosslinks that are typically assumed to react with the environment so that degradation can be measured by the decrease in crosslink density, which is unrepresentative of highly-crosslinked epoxy/amine resins. Li *et al*. [26] proposed a model for hydrogels considering chain scission rather than crosslink breakage, where the Flory-Rehner equation is coupled with a first-order kinetics law to produce a statistical model for swelling caused by the degradation of poly(ethylene glycol) with different chain lengths. Gilormini *et al*. [27] focused on crosslinked polymers rather than hydrogels, and although they used the affine network assumption to estimate the elastic shear modulus from crosslink density, they also assumed crosslinks as the primary reaction site, which is applicable to anhydride-cured epoxy. Advances in molecular modelling technology have prompted an increase in numerical analysis studies of elastic properties of soft networks [31–33], but only one model focused on the effect of water on the elastic modulus of thin polymer films [34].

There are currently no analytical models which can directly relate the local chemical environment and polymer structure to the bulk network elastic properties – *i.e.*, elastic properties in the damaged state, where chain scission is the degradation mechanism. This paper presents such a model for the service life prediction of amine-crosslinked bisphenol-based epoxy materials used in acid environments, only requiring five parameters: crosslink density and chain functionality (measurable), penetration rate and equilibrium acid uptake (measurable), and reaction rate constant (approximated by fitting).

2. Experimental study

2.1. Materials

The model epoxy resin used in this study was a mixture of bisphenol-F epoxy (DGEBF, Epiclon 830, $M_w \sim 320$) and poly(ether)amine (PEA, Jeffamine D230, $M_w \sim 230$). These monomers react to form a crosslinked network with tertiary amine crosslinks and a mixture of aliphatic and aromatic ethers. DGEBF and PEA were mixed with a 100:33.4 ratio by weight, degassed and oven-cured at 80 °C for 24 hr and 120 °C for 24 hr, from which rectangular specimens with dimensions of 60×20×2 mm^3 were cut using a water-cooled silicon carbide blade.

2.2. Experimental procedure

In applications where epoxy resin is exposed to aqueous acid, only chemical tanks would constitute a case of highly-concentrated acid, whereas service conditions for epoxy linings or other structural applications would involve low concentrations. Aqueous H_2SO_4 at concentrations of 0.1, 1.0, and 10 wt% and temperatures of 60 and 80 °C were selected as model environmental conditions, in which specimens were immersed for various durations, and the acid penetration was monitored by measuring the change in mass. At several durations, the immersed specimens were dried in vacuum until the mass stabilized (usually several weeks to months), then recorded as the 'dry' state. This was done to approximate the actual water-free acid uptake. Previous studies have shown that the penetration depth of H_2SO_4 in amine-cured epoxy as measured elemental sulfur mapping by EDS can be accurately represented by the mass change since it does not exhibit a Fickian concentration gradient [4, 14]. FTIR was also used to identify degradation, as mentioned in detail in previous work [19].

Strength is dependent on various factors, including defects and stress concentrations, making it difficult

to control the scatter with a small sampling size; thus, the elastic modulus was chosen as the mechanical property to assess chemical damage by acid. Water can significantly affect the elastic modulus, convoluting the effects of polymer network damage, so the elastic modulus was measured on dried specimens by three-point bending on an electromechanical testing machine at a crosshead speed of 1 mm/min and span length of 40 mm (ASTM D790). The tangent modulus of elasticity E_b for a rectangular cross-section is given by [35] (Equation (1)):

$$E_b = \frac{L^3 m}{4bd^3} \tag{1}$$

where L is the span length, b is the specimen width, d is the specimen thickness, and m is the slope of the linear portion of the force-deflection curve (*i.e.*, at small strains).

2.3. Results

The mass uptake behavior of H_2SO_4 is shown for the wet and dry conditions in Figure 1. There seems to be insignificant influence of temperature on equilibrium uptake, which is primarily determined by acid concentration. However, the diffusion rate is expectedly temperature-dependent. Note that the dry condition represents an estimation of penetrated acid, which is hereafter the assumed state when discussing mass change.

Although the gravimetric profiles resemble Fickian diffusion behavior, EDS elemental mapping of sulfur ions confirms a sharp concentration gradient that invalidates the underlying assumptions of Fick's second law [4, 14] (Equation (2)):

$$\frac{\mathrm{d}c}{\mathrm{d}t} = D\frac{\partial^2 t}{\partial x^2} \tag{2}$$

where c is the concentration of penetrant in the material thickness dimension x, D is the diffusivity, and t is time. This integrates to the approximate solution [36] (Equation (3)):

$$\frac{M_t}{M_\infty} = 1 - \frac{8}{\pi^2}\sum_{n=0}^{\infty}\frac{1}{(2n+1)^2}\exp\left(\frac{-D(2n+1)^2\pi^2 t}{4h^2}\right) \tag{3}$$

For curve-fitting purposes, this mathematical form of the approximate solution to Fick's second law is convenient for obtaining an approximate diffusivity D. However, using the relation $x_A = M_A/M_{\infty,A}$ to define the penetration depth for inorganic acids, a simple approximation for x_A at time t the Equation (4):

$$x_A = D_A t^{1/2} \tag{4}$$

where D_A is the penetration rate coefficient (units of $hr^{-1/2}$). Figure 2 summarizes the acid uptake behavior in terms of equilibrium mass change (after drying) $M_{\infty,A}$, D and D_A, all of which increase with acid concentration in a similar way to that reported in previous work [2, 4, 7]. Higher temperature increases D_A as expected, but no significant difference can be seen for $M_{\infty,A}$ except for a small increase in the case of 10 wt%. These two parameters are largely responsible for controlling the progression and maximum level of damage in the polymer.

FTIR spectra – taken from dry specimens after reaching equilibrium in different acid concentrations – suggest that a small amount of aryl ether cleavage (resulting in phenol and aldehyde) takes place [19–21], providing a pathway for chain scission that does not involve amine crosslinks (Figure 3a). A small peak is visible that indicates some unreacted epoxide groups are present, but this does not change noticeably during immersion, and excess epoxy has a smaller influence on the proton reactions than excess amine (see Section 3). Therefore, we did not consider this to be a problem. The photographs in Figure 3b

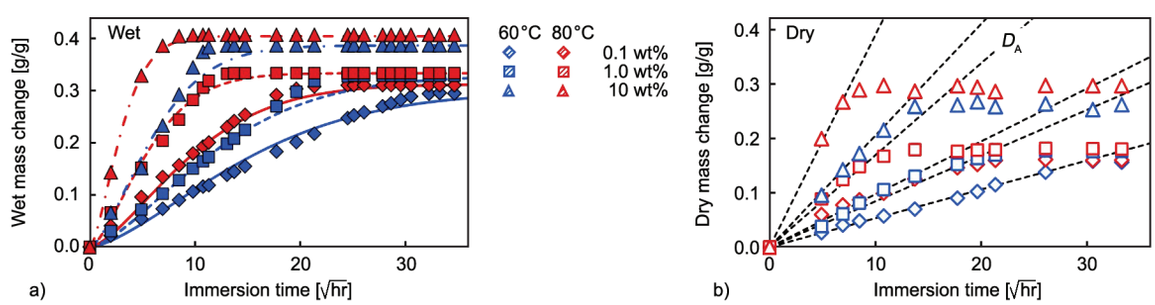

Figure 1. Acid penetration behavior for various H_2SO_4 concentrations, in the wet (a) and dry (b) conditions.

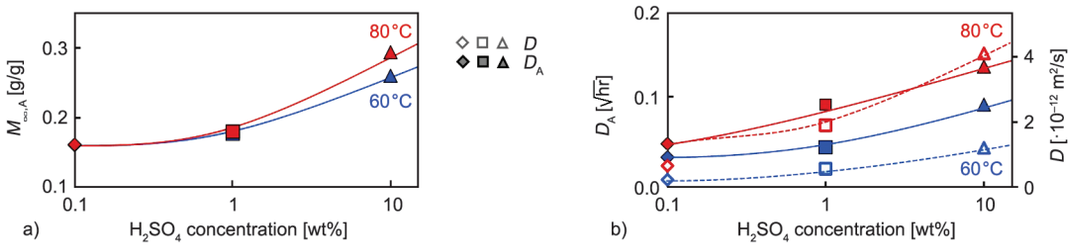

Figure 2. Equilibrium mass change (a) and diffusivity (b) for different conditions (The lines are only intended to help the eye).

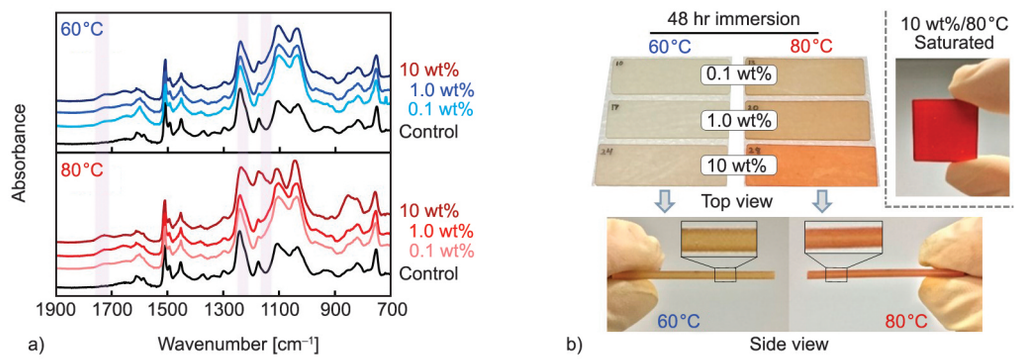

Figure 3. Chemical changes in acid-immersed epoxy shown by (a) FTIR analysis of carbonyl and ether groups, and (b) photographs of significant color change and visible penetration layer.

of specimens after 48 hr of immersion reveal visual changes indicative of penetration and reaction by sulfuric acid; the once-colorless epoxy turns red as the reaction progresses. Furthermore, the distinct penetrated layer is clearly visible even to the eye (inset). Figure 4a shows representative force-deflection curves of the control (pristine) epoxy and degraded epoxy after drying. The slope m was taken in the linear region (<2 mm) and used to calculate the tangent modulus in Equation (1). Evidence of reaction kinetics-dominated damage progression is shown in Figure 4b, where the residual modulus shows no decrease even after a significant amount of acid has penetrated the epoxy (acid uptake ~7%), until a reduction occurs – gradually in the case of low concentrations, and abruptly in the case of high concentrations. Temperature does not appear to influence the overall damage mechanism since all data from both temperatures follow the same trend, but the rate should be affected by temperature according to Arrhenius kinetics. These experimental results, in continuation with the experimental and analytical results in Tanks *et al*. [19], form the basis for the key analytical model development in Section 3.

3. Analysis of network damaged by acid

This section presents a theoretical investigation of the mechanical damage that occurs in amine-cured bisphenol-diglycidylether epoxy systems as a result of inorganic acid penetration; *i.e*., we present an analytical model for relating acid uptake behavior to reductions in elastic properties.

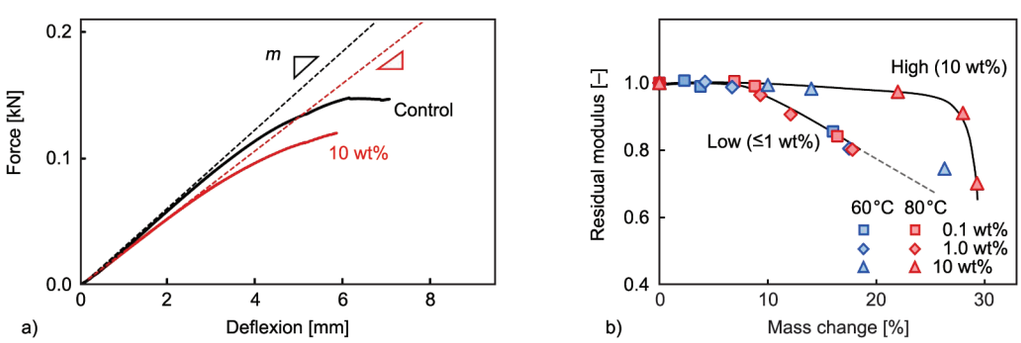

Figure 4. Flexural properties of pristine and degraded DGEBF/amine networks: (a) typical force-deflection curves showing the approximation method of the tangent modulus, and (b) normalized modulus as a function of dry mass change.

3.1. Key assumptions

Following the work in Tanks *et al*. [19], there are several simplifying assumptions that must be made for the current model:

(1) The crosslinked structure is ideal; *i.e*., no loops or uncured functional groups, so that every crosslink point is a tertiary amine and there are no epoxy chain having both ends connected to the same amine chain.
(2) Reactions occur randomly in the acid penetrated layer (no biased direction).
(3) Based on the crosslink density, the threshold environmental acid concentration needed to satisfy only the amine protonation reaction is 0.009 M (corresponding to an equilibrium mass change of ~12%), so any excess acid above this contributes to chain scission through ether cleavage. Thus, the selected concentrations of 0.1, 1.0 and 10 wt% (0.019, 0.189 and 1.889 M, respectively) are assumed to cause chain scission of different degrees.
(4) Amine crosslinks are protonated by acid but do not break; aryl ether cleavage is the primary mechanism of chain scission.
(5) The polymer network is affine in both the initial and damaged states, such that elastic properties can be estimated from network structure using the Gaussian phantom network theory [27].

Figure 5 illustrates the network structure and degradation process described by this 2D analysis, where polyetheramine (PEA) and bisphenol-F diglycidyl-ether monomers constitute a model epoxy system.

3.2. Network features

Features of the network structure considered for the degradation model by inorganic acid [19] are described in more detail here. Consider an ideal 2D crosslinked network, represented by a unit cell with n nodes and dimensions $a \times b$ (out-of-plane thickness is unity), as shown in Figure 6. This unit cell is sufficiently large that assumption #2 is valid and that the calculation of mechanical properties is not affected by boundary conditions or damage distribution. The crosslink density ν can be expressed as (Equation (5)):

$$\nu = \frac{n}{ab} \tag{5}$$

The density of elastically effective chain connections – meaning the number of load-bearing chains connected to each crosslink per unit volume – is given by Equation (6):

$$\nu_c = \frac{3n}{ab} \tag{6}$$

for diamine crosslinker, which is tetra-functional (*i.e*., a maximum of two epoxy segments connected to each amine). From assumption #1, it follows that

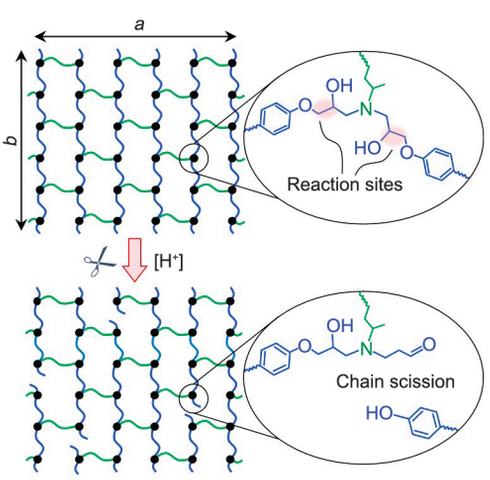

Figure 6. Schematic of ideal 2D network damage process, consisting of alcohol elimination followed by aryl ether cleavage in a H_2SO_4 environment.

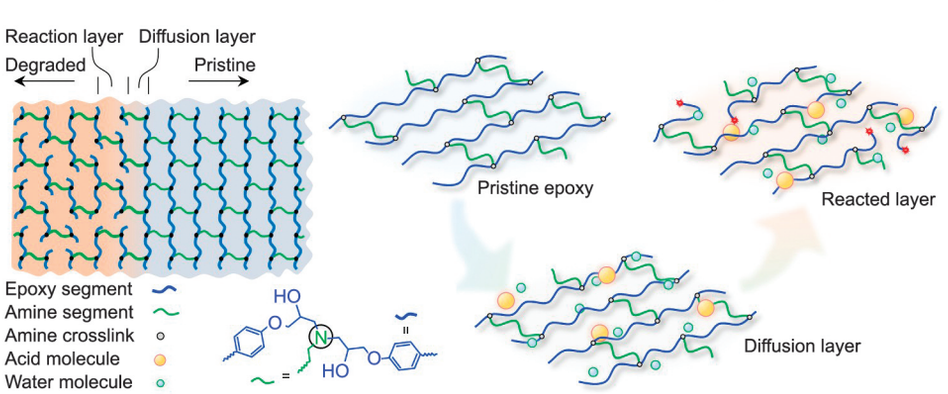

Figure 5. Model system comprised of an ideal 2D network undergoing layer-wise penetration and degradation by acid. Each crosslink consists of a tertiary amine (NR_3), two secondary alcohols (ROH) and two aryl ethers (ROR).

the number of elastically effective chain density – the number of load-bearing chains per unit volume –can be approximated by Equation (7):

$$n_c \approx \frac{1}{2}\nu_c \tag{7}$$

for the initial state only. The relationship between n_c and ν_c no longer holds once damage is present; Equations (6) and (7) are used for relating the elastic modulus in the initial state to the chain density rather than crosslink density since n is assumed to be constant. Using the affine network assumption [27, 32, 37], the elastic modulus in the initial state E_0 can be related to crosslink density by Equation (8):

$$E_0 = 3\nu RT \tag{8}$$

where R is the universal gas constant and T is the temperature. To calculate the elastic modulus in the damaged state, we used chain density instead of crosslink density (Equation (9)):

$$E_0 = 3nL_cRT \tag{9}$$

3.3. Degree of degradation at local equilibrium

Because the degree of degradation is represented as a statistical average per crosslink site, the expression for local degradation in the penetrated layer comes from Equation (6) (Equation (10)):

$$\hat{\nu}_c = \frac{n(3 - f_{ROR})}{ab} \tag{10}$$

where f_{ROR} is the average number of chain scission reactions that can occur given a certain amount of available acid (H^+), which follows from Equation (11), (12) [19]:

$$\nu_{exp} = \frac{M_{\infty,A}\rho_0}{m_A}\frac{a_H}{\bar{f}} \tag{11}$$

$$f_{ROR} = \frac{1}{2}\left(\frac{M_{\infty,A}\rho_0}{m_A}\frac{a_H}{\nu_{exp}} - 1\right) \tag{12}$$

where ν_{exp} is the experimentally determined crosslink density, $M_{\infty,A}$ is the equilibrium acid uptake by mass (excluding water), a_H is the number of dissociated protons per acid molecule, mA is the molecular weight of the acid, and ρ_0 is the initial polymer density. The total functionality of the unit cell $\bar{f} = f_{R_3N}) + f_{OH} + f_{ROR}$ is the summation of reactive sites: amine, alcohol, and ether (respectively). Chain scission is proposed to occur at the aryl ethers in the bisphenol epoxy segment, according to previous work [19–21], where f_{ROR} accounts for the presence of aliphatic ethers in the amine segment.

The approximate degraded elastic modulus in the penetrated layer can be written by combining Equations (9) and (10) (Equation (13)):

$$\hat{E} = 2\hat{n}_cRT \tag{13}$$

which can be normalized by the initial modulus to yield (Equation (14)):

$$\frac{\hat{E}}{E_0} = \frac{\hat{n}_c}{n_c} \tag{14}$$

The bulk material properties – as measured experimentally – in the damaged state can be approximated as the average of $\hat{E}$ and E_0 proportional to their respective volumes. Thus, the global normalized elastic modulus can be written as (Equation (15)):

$$\frac{E}{E_0} = \frac{\hat{n}_c}{n_c}x_A + (1 - x_A) \tag{15}$$

which finally reduces to (Equation (16)):

$$\frac{E}{E_0} = 1 - \frac{f_{ROR}}{3}x_A \tag{16}$$

where $x_A = M_A/M_{\infty,A}$ represents the relative penetration depth of the acid.

3.4. Reaction kinetics and penetration rate

The previous section describes the model for predicting the elastic modulus in the damaged state at equilibrium (*i.e.*, all reactions have been completed). However, at short times the penetration rate of the acid may be much higher than the chain scission rate, such that the penetrated layer is not immediately degraded. This is clearly observed in the experimental data (Figure 4b), since the residual modulus does not decrease linearly with acid uptake starting at $t = 0$. Therefore, a kinetic model is required to adequately capture the complex degradation process. In this work, a pseudo-first order reaction kinetics law is assumed, using the parameter f_{ROR} to signify the reactive species (Equation (17)):

$$\frac{d[f_{ROR}]}{dt} = -k[f_{ROR}][A]_0 = -\bar{k}[f_{ROR}] \tag{17}$$

where k is the second order reaction rate constant; the concentration of acid [A] is assumed to be essentially constant due to the external source, leading to the use of a new pseudo-first order rate constant $\bar{k}$. The probability that a reactive chain remains intact is (Equation (18)):

$$\frac{[f_{ROR}]}{[f_{\mathrm{ROR}}]_0} = \exp(-\bar{k}t) \tag{18}$$

This leads to the expression for the extent of reaction ξ_i within penetrated layer i (Equation (19)):

$$\xi_{\mathrm{i}} = 1 - \exp(-\bar{k}\tau) \tag{19}$$

where τ is the reaction time – also referred to as the dwell time. It starts counting once layer i has been fully penetrated at time t_i (meaning $\tau_j = t_{i+1}$), with increment size equal to the global time increment (*i.e.*, penetration time) so that $\Delta\tau = \Delta t$. Equation (16) can then be rewritten to express the extent of reaction in layer i (penetrated at time t_i) at dwell time increment i as Equation (20):

$$\xi_{\mathrm{i}}^{\mathrm{j}} = 1 - \exp\left(-\bar{k}\tau_{\mathrm{j}}\right) \tag{20}$$

The acid continues to penetrate the polymer during this time period. Thus, the elastic modulus of layer i in the damaged state at time t_{i+1} is Equation (21):

$$\left(\frac{\hat{E}_{\mathrm{i}}}{E_0}\right)_{\mathrm{j}} = \left(1 - \frac{f_{\mathrm{ROR}}}{3}\right)\xi_{\mathrm{i}}^{\mathrm{j}} = \left(1 - \frac{f_{\mathrm{ROR}}}{3}\right)\left[1 - \exp\left(-\bar{k}[t_{\mathrm{i+k}} - t_{\mathrm{i}}]\right)\right] \tag{21}$$

which is the specific expression for thermodynamically-bounded local value at any point in time in a one-dimensional system.

Now we must select an appropriate model to describe the acid penetration behavior, since this accounts for the reactant supply in Equation (17). As discussed in Sections 2.2 and 3.2, there is sufficient experimental evidence confirming that inorganic acids do not follow Fick's laws [4, 14, 18]. While it is trivial to fit the mass uptake data with an arbitrary function that serves as the input to Equation (20), there are several phenomenological models available in the literature for diffusion-reaction systems. Borrowing from the concept of bound and mobile water molecules in the so-called Langmuir-type diffusion model [36, 38], we speculate that acid molecules may be mobile or bound ('trapped') in polar sites within the global penetration scheme. Consider that the total acid uptake is comprised of bound and mobile acid molecules whose concentration follows a power-law (Equations (22), (23)):

$$M_{\mathrm{A,\,b}} = f(M_{\mathrm{A}}) = (M_{\mathrm{A}})^{\beta} \tag{22}$$

$$M_{\mathrm{A,\,m}} = M_{\mathrm{A}} - M_{\mathrm{A,\,b}} \tag{23}$$

where $\beta \geq 1$ is a concentration-dependent shape parameter. There is currently no experimental evidence in the literature that confirms or denies this behavior – we simply propose a possible explanation for the observed concentration dependency.

3.5. Elastic modulus of a layer-wise degraded beam

In the case of uniaxial tensile loading, the local elastic modulus in Equation (21) can be homogenized across the bulk volume of the polymer (having m layers) at time t_i to give Equation (24):

$$\left(\frac{E_{\mathrm{i}}}{E_0}\right)_{\mathrm{j}} = \sum_{\mathrm{i}=1}^{\mathrm{m}} \left(\frac{\hat{E}_{\mathrm{i}}}{E_0}\right)_{\mathrm{j}} \tag{24}$$

However, our study employs a simply supported three-point bending test to evaluate the elastic modulus, so a flexural analysis of layered beams after Bîrsan *et al*. [39] is more accurate. The equivalent flexural stiffness for the structure shown in Figure 7a can be expressed as Equation (25):

$$(EI)_{\mathrm{eq}} = \frac{1}{3}\sum_{\mathrm{i}=1}^{\mathrm{n}}\left(y_{\mathrm{i}}^3 - y_{\mathrm{i+1}}^3\right) - \frac{\left(\frac{1}{2}\sum_{i=1}^{n}\left(y_i^2 - y_{i+1}^2\right)\right)^2}{\sum_{i=1}^{n}(y_i - y_{i+1})E_i} \tag{25}$$

where y_i is the distance from the neutral axis of the beam to the penetrated layer i. The elastic modulus can then be estimated by the layer-wise summation of stiffnesses at each time increment and normalizing by the moment of inertia I. Since the degradation begins on the outer surface and progresses inward, the pristine epoxy stiffness is continually reduced while being symmetrical around the neutral axis. This means that the global modulus calculated by Equation (25) will be slightly lower than Equation (24) at intermediate durations (*i.e.*, they are the same at $t = 0$ and equilibrium). As a result, the predictions are conservative.

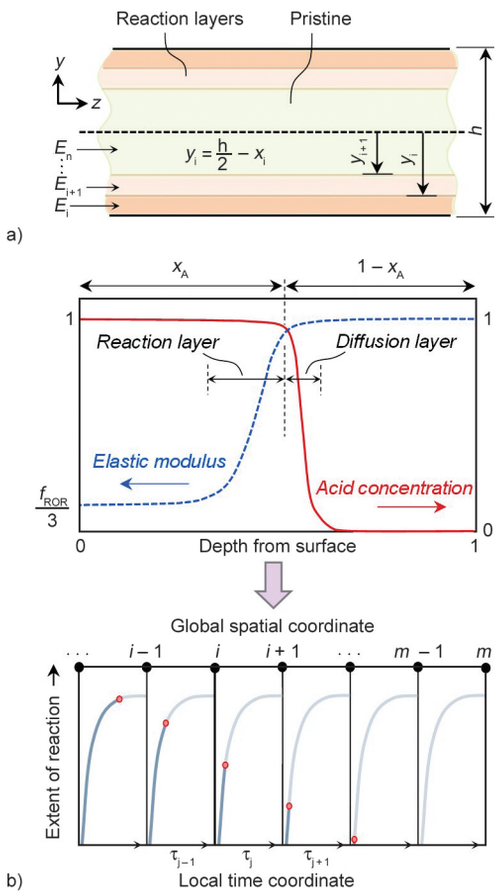

Figure 7. Scheme to solve for the reaction variable and residual elastic modulus through the thickness in the case of layer-wise acid penetration: (a) schematic of the layered beam model, and (b) schematic of 1D reaction model.

The model was solved using a 1D central difference scheme written in python, as illustrated in Figure 7b. Assuming penetration occurs only through the thickness of the epoxy, the body was divided into layers in which the reaction only begins once the acid has fully penetrated (t_i), at which point the reaction progresses through each time step (τ_j) until complete.

4. Analysis results

4.1. Instantaneous scission vs kinetic scission

The kinetic behavior described by Equation (19) is demonstrated in Figure 8a for various values of $\bar{k}$, such that a higher value equates to a shorter time until the layer is fully reacted (*i.e.*, maximum damage). It is extremely difficult to isolate the reactions that occur in a polymer system to measure the reaction rates of that functional group alone accurately; we refer to other studies [20, 21] on acid cleavage of aryl ethers to approximate the general range of $\bar{k}$ values, which appears to be around 0.008–0.1 hr^{-1}. For faster reaction rates, the reaction in a given layer will reach completion faster, until the reacted region is nearly equivalent to the penetrated region at a given time. This can be considered instantaneous scission, wherein the change in mechanical properties of the network is directly proportional to acid uptake; this was not experimentally observed for the H_2SO_4 concentrations in this study. Numerical examples of $M_A = M_{A,b} + M_{A,m}$ are shown in Figure 8b, 8c. As

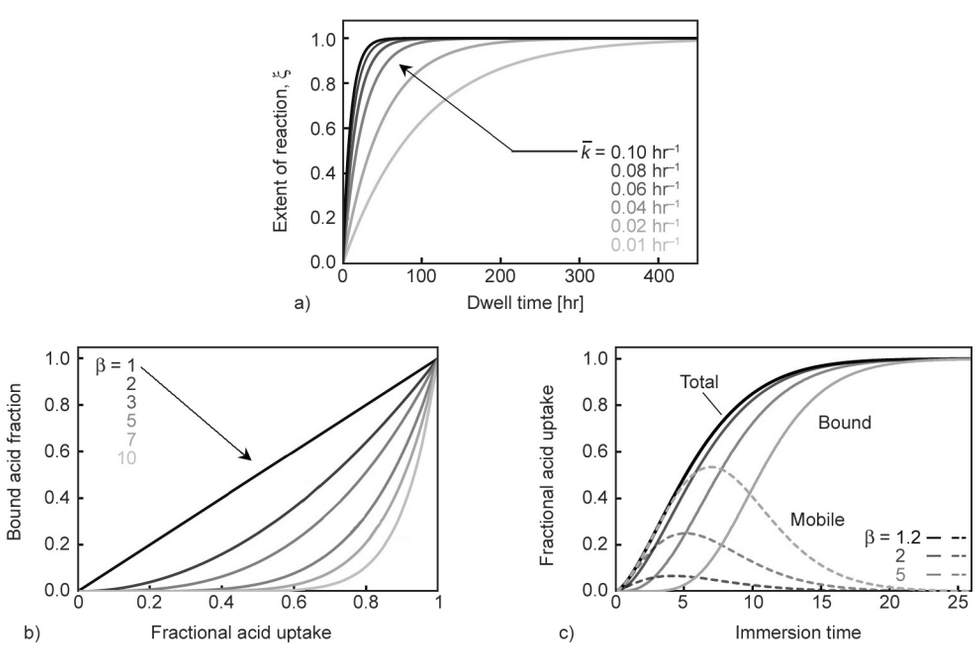

Figure 8. (a) Relationship between rate constant $\bar{k}$ and extent of reaction ξ, (b) influence of shape parameter β on the fraction of bound acid, and (c) example of decomposed acid uptake curve into bound and mobile concentrations.

β increases, the relative portion of bound acid molecules – available for reaction – becomes delayed at short timescales and accelerated at longer ones. The combination of concentration-dependent diffusion and reaction leads to a flexible model for capturing various complex mechanisms.

4.2. Degraded network properties

We found that for high acid concentrations (10 wt%), the modulus was maintained until a higher degree of acid penetration before suddenly falling, compared to the more gradual decline seen with low concentrations (Figure 4b). However, as higher concentration would not exhibit lower reaction rates than lower concentrations, we must assume that the local acid concentration and proton activity is different for higher concentrations due to significantly higher penetration rates and stoichiometric changes [18]. Thus we consider different values of β to explain the disparity between experiment and analysis for a given rate constant.

Model predictions are plotted against experimental data in Figure 9, showing good agreement using the best-fit parameters of $\bar{k}$ in Table 1 (crosslink density for the model polymer is taken [19] as ν_{exp} = 1.621 mol/cm^3). The model appears particularly valid for low concentrations, using rate constants similar to those in the literature. Higher concentrations present a challenge for the model when calculating acid concentration *vs* penetration depth via Equation (4), since the comparatively high penetration rate quickly initiates the reaction at short durations (*i.e.*, <10 hr); however, based on experimental data, we propose that the reaction takes more time to initiate so that the reaction time becomes relatively smaller as the system approaches equilibrium (*i.e.*, long durations). Thus, the selected function in Equation (22) shows better agreement with experiments by dividing the local concentration of protons in early-stage penetrated layers into bound and mobile species. A more sophisticated physiochemical model is needed to describe this complex diffusion/reaction behavior accurately. Using the information on the network structure (ν_{exp},

Table 1. Model parameters for DGEBF/PEA system degraded by H_2SO_4.

Parameter	0.1 wt%		1.0 wt%		10 wt%	
	60 °C	80 °C	60 °C	80 °C	60 °C	80 °C
$M_{\infty,A}$ [%]	15.6	15.9	17.6	18.0	26.1	26.7
f_{ROR} [–]	0.457	0.476	0.642	0.662	0.865	0.934
$\bar{k}$ [hr^{-1}]	0.019	0.028	0.037	0.058	0.046	0.092
D_A [hr$^{-1/2}$]	0.033	0.048	0.044	0.080	0.091	0.133

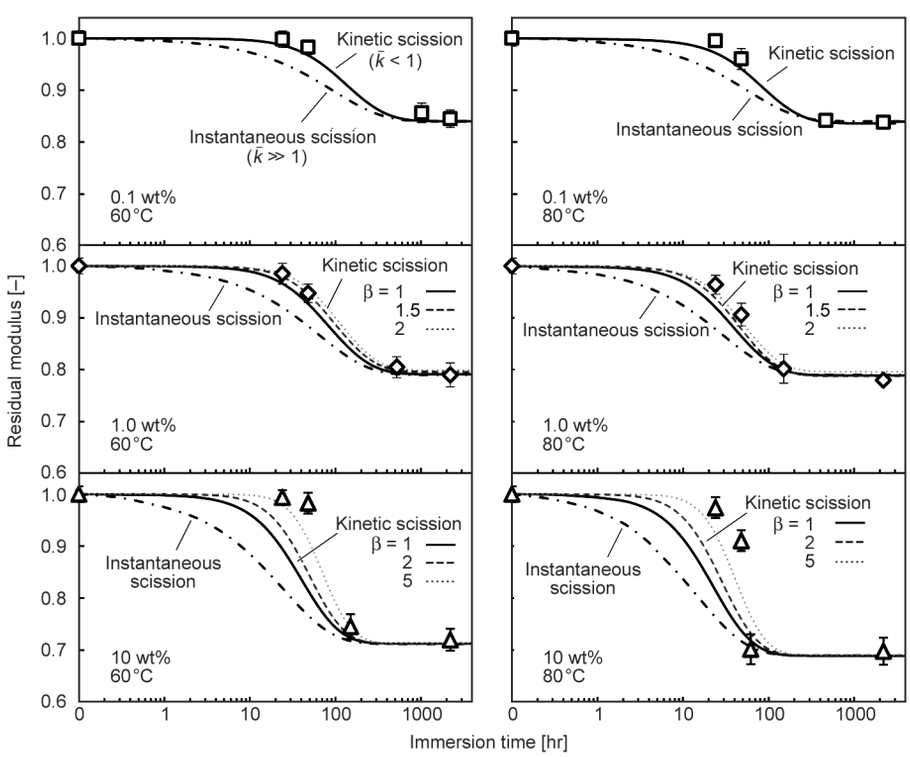

Figure 9. Model predictions of residual elastic modulus during exposure to H_2SO_4 at various concentrations and temperatures, comparing instantaneous *vs.* kinetic for different values of β.

f_{ROR}), this model directly predicts the change in elastic properties based on a specific reaction mechanism.

As mentioned above, the reaction rate constants $\bar{k}$ and activation energies E_a – 16.3, 22.0, and 33.9 kJ/mol for 0.1, 1.0, and 10 wt%, respectively – corresponding to the model were obtained by fitting the experimental data. However, this study demonstrates the utility of our network analysis approach for relating chemical processes to mechanical properties; although we did not find comparable data in the literature, they follow pseudo-first order kinetics and appear valid (Figure 10). Future work will include a wider range of temperatures, acid types, and network structures. For example, weak organic acids present a difficult challenge due to their typically higher *pKa* values and solvent swelling properties, so the effects of swelling stresses would need to be incorporated in the stiffness formulation. As for different epoxy networks, a mixed-hardener system involving polyamides or esters would constitute a different reaction scheme, complicating the determining of rate constants. However, by systematically varying the chemical structure and employing the basic approach of our model, it would be possible to formulate the specific expression relating reaction schemes to mechanical properties. In the future, a random 3D model will replace the ideal 2D model to reflect the connectivity (elastic chain density) more accurately. This will require automated node and edge generation, which was outside the scope of the current paper.

5. Conclusions

Experimental investigations revealed a layer-wise penetration process of inorganic acid (H_2SO_4) in amine-cured epoxy resin, accompanied by physical damage manifested in reduced elastic properties. A mechanistic model was proposed for relating the environmental conditions and polymer structure to the long-term elastic properties of an amine-crosslinked phenolic epoxy resin, based on a simple 2D network analysis. The only fitting parameter in this model is the reaction rate constant $\bar{k}$, which is difficult to determine directly through isolated experiments, but the best-fit values were within the ranges for aryl ether cleavage in the literature. The analytical results show good agreement with experimental data. We show that features of the network structure such as functionality and crosslink density determine the equilibrium damaged state, while the degradation kinetics are primarily influenced by the penetration and reaction rates. This framework can be used for other material-environment systems that exhibit coupled diffusion-reaction damage processes, given that the degradation mechanism is understood. Furthermore, it serves as a 'black box' for approximating reaction rate constants in complex networks if the inputs (*i.e.*, polymer structure, environmental conditions) and outputs (*i.e.*, mechanical properties, spectroscopic analyses) are known since direct measurement is unfeasible. Extending this model to 3D random networks with partial curing effects would be particularly useful for large-scale numerical simulations of thermosetting resins and their composites in applications such as automotive, pipeline, and aerospace structures.

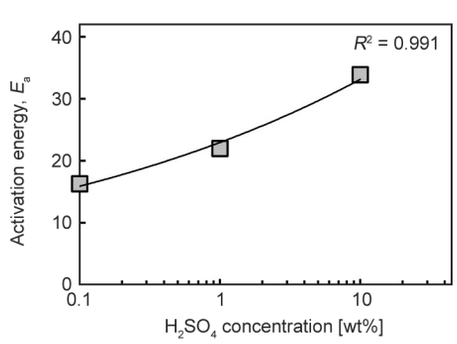

Figure 10. Approximated activation energy E_a for increasing H_2SO_4 concentrations.

Acknowledgements

J. T. acknowledges the financial support of the Ministry of Education, Culture, Sports, Science and Technology (MEXT) Japan.

References

[1] Møller V. B., Dam-Johansen K., Frankær S. M., Kiil S.: Acid-resistant organic coatings for the chemical industry: A review. Journal of Coatings Technology and Research, **14**, 279–306 (2017). https://doi.org/10.1007/s11998-016-9905-2

[2] Sembokuya H., Negishi Y., Kubouchi M., Tsuda K.: Corrosion behavior of epoxy resin cured with different amount of hardener in corrosive solutions. Journal of the Society of Materials Science Japan, **9**, 230–234 (2003). https://doi.org/10.2472/jsms.52.9Appendix_230

[3] Tsuda K.: Behavior and mechanisms of degradation of thermosetting plastics in liquid environments. Journal of the Japan Petroleum Institute, **50**, 240–248 (2007). https://doi.org/10.1627/jpi.50.240

[4] Abacha N., Kubouchi M., Tsuda K., Sakai T.: Performance of epoxy-nanocomposite under corrosive environment. Express Polymer Letters, **1**, 364–369 (2007). https://doi.org/10.3144/expresspolymlett.2007.51

[5] Frank K., Childers C., Dutta D., Gidley D., Jackson M., Ward S., Maskell R., Wiggins J.: Fluid uptake behavior of multifunctional epoxy blends. Polymer, **54**, 403–410 (2013). https://doi.org/10.1016/j.polymer.2012.11.065

[6] Pitarresi G., Toscano A., Alessi S.: Fracture toughness of synthesized high-performance epoxies subject to accelerated water aging. Polymer Testing, **68**, 248–260 (2018). https://doi.org/10.1016/j.polymertesting.2018.04.010

[7] Padarthi Y., Mohanta S., Gupta J., Neogi S.: Quantification of swelling stress induced mechanical property reduction of glass fiber/epoxy composites immersed in aqueous 10% sulphuric acid by instrumenting with distributed optical fiber sensors. Fibers and Polymers, in press (2021). https://doi.org/10.1007/s12221-021-0317-2

[8] El Yagoubi J., Lubineau G., Traidia A., Verdu J.: Monitoring and simulations of hydrolysis in epoxy matrix composites during hygrothermal aging. Composites Part A: Applied Science and Manufacturing, **68**, 184–192 (2015). https://doi.org/10.1016/j.compositesa.2014.10.002

[9] Capiel G., Miccio L. A., Montemartini P. E., Schwartz G. A.: Water diffusion and hydrolysis effect on the structure and dynamics of epoxy-anhydride networks. Polymer Degradation and Stability, **143**, 57–63 (2017). https://doi.org/10.1016/j.polymdegradstab.2017.06.010

[10] Capiel G., Uicich J., Fasce D., Montemartini P. E.: Diffusion and hydrolysis effects during water aging on an epoxy-anhydride system. Polymer Degradation and Stability, **153**, 165–171 (2018). https://doi.org/10.1016/j.polymdegradstab.2018.04.030

[11] Barkoula N. M., Karabela M., Zafeiropoulos N. E., Tsotra P.: Fast curing versus conventional resins – Degradation due to hygrothermal and UV exposure. Express Polymer Letters, **14**, 401–415 (2020). https://doi.org/10.3144/expresspolymlett.2020.34

[12] Zhang A. Y., Li D. H., Zhang D. X., Lu H. B., Xiao H. Y., Jia J.: Qualitative separation of the effect of voids on the static mechanical properties of hygrothermally conditioned carbon/epoxy composites. Express Polymer Letters, **5**, 708–716 (2011). https://doi.org/10.3144/expresspolymlett.2011.69

[13] Chow W. S.: Water absorption of epoxy/glass fiber/organo-montmorillonite nanocomposites. Express Polymer Letters, **1**, 104–108 (2007). https://doi.org/10.3144/expresspolymlett.2007.18

[14] Kusano M., Kubouchi M., Bulgarevich D. S., Shiwa M.: Non-destructive evaluation by terahertz spectroscopy for penetration of acid solutions into epoxy resin. Express Polymer Letters, **10**, 941–949 (2016). https://doi.org/10.3144/expresspolymlett.2016.87

[15] Dang W., Kubouchi M., Sembokuya H., Tsuda K.: Chemical recycling of glass fiber reinforced epoxy resin cured with amine using nitric acid. Polymer, **46**, 1905–1912 (2005). https://doi.org/10.1016/j.polymer.2004.12.035

[16] Dang W., Kubouchi M., Yamamoto S., Sembokuya H., Tsuda K.: An approach to chemical recycling of epoxy resin cured with amine using nitric acid. Polymer, **43**, 2953–2958 (2002). https://doi.org/10.1016/S0032-3861(02)00100-3

[17] Hanaoka T., Arao Y., Kayaki Y., Kuwata S., Kubouchi M.: Analysis of nitric acid decomposition of epoxy resin network structures for chemical recycling. Polymer Degradation and Stability, **186**, 109537 (2021). https://doi.org/10.1016/j.polymdegradstab.2021.109537

[18] Lim J. S. K., Gan C. L., Hu X. M.: Unraveling the mechanistic origins of epoxy degradation in acids. ACS Omega, **4**, 10799–10808 (2019). https://doi.org/10.1021/acsomega.9b00859

[19] Tanks J., Kubouchi M., Arao Y.: Influence of network structure on the degradation of poly(ether)amine-cured epoxy resins by inorganic acid. Polymer Degradation and Stability, **157**, 153–159 (2018). https://doi.org/10.1016/j.polymdegradstab.2018.10.011

[20] Sturgeon M. R., Kim S., Lawrence K., Paton R. S., Chmely S. C., Nimlos M., Foust T. D., Beckham G. T.: A mechanistic investigation of acid-catalyzed cleavage of aryl-ether linkages: Implications for lignin depolymerization in acidic environments. ACS Sustainable Chemistry and Engineering, **2**, 472–485 (2014). https://doi.org/10.1021/sc400384w

[21] Jasiukaitytė-Grojzdek E., Huš M., Likozar B.: Acid-catalyzed α-O-4 aryl-ether cleavage mechanisms in (aqueous) γ-valerolactone: Catalytic depolymerization reactions of lignin model compound during organosolv pretreatment. ACS Sustainable Chemistry and Engineering, **8**, 17475–17486 (2020). https://doi.org/10.1021/acssuschemeng.0c06099

[22] Shaw M. T.: Models of a degrading polymer network. Journal of Chemical Physics, **54**, 2172–2177 (1971). https://doi.org/10.1063/1.1675149

[23] Metters A. T., Anseth K. S., Bowman C. N.: A statistical kinetic model for the bulk degradation of PLA-*b*-PEG-*b*-PLA hydrogel networks: Incorporating network non-idealities. Journal of Physical Chemistry B, **105**, 8069–8076 (2001). https://doi.org/10.1021/jp004083h

[24] Metters A., Hubbell J.: Network formation and degradation behavior of hydrogels formed by Michael-type addition reactions. Biomacromolecules, **6**, 290–301 (2005). https://doi.org/10.1021/bm049607o

[25] Reddy S. K., Anseth K. S., Bowman C. N.: Modeling of network degradation in mixed step-chain growth polymerizations. Polymer, **46**, 4212–4222 (2005). https://doi.org/10.1016/j.polymer.2005.02.050

[26] Li X., Kondo S., Chung U-I., Sakai T.: Degradation behavior of polymer gels caused by nonspecific cleavages of network strands. Chemistry of Materials, **26**, 5352–5357 (2014).
https://doi.org/10.1021/cm502480f

[27] Gilormini P., Richaud E., Verdu J.: A statistical theory of polymer network degradation. Polymer, **55**, 3811–3817 (2014).
https://doi.org/10.1016/j.polymer.2014.05.008

[28] Escobar F., Anseth K. S., Schultz K. M.: Dynamic changes in material properties and degradation of poly (ethylene glycol)-hydrazone gels as a function of pH. Macromolecules, **50**, 7351–7360 (2017).
https://doi.org/10.1021/acs.macromol.7b01246

[29] Jahanmir G., Abdekhodaie M. J., Chau Y.: Stochastic modeling of degradation behavior of hydrogels. Macromolecules, **51**, 3941–3952 (2018).
https://doi.org/10.1021/acs.macromol.8b00165

[30] Machatschek R., Saretia S., Lendlein A.: The interplay between network morphology and degradation kinetics of polymers: Theoretical and experimental analysis by means of a 2D model system. MRS Advances, **5**, 679–691 (2020).
https://doi.org/10.1557/adv.2019.457

[31] Liu S., Wang P., Huang G., Wang L., Zhou J., Lu T. J., Xu F., Lin M.: Reaction-induced swelling of ionic gels. Soft Matter, **5**, 449–455 (2015).
https://doi.org/10.1039/C4SM02252A

[32] Heidemann K. M., Sharma B., Rehfeldt F., Schmidt C. F., Wardetzky M.: Elasticity of 3D networks with rigid filaments and compliant crosslinks. Soft Matter, **11**, 343–354 (2015).
https://doi.org/10.1039/C4SM01789G

[33] Kawai R., Tanaka H., Matsubara S., Ida S., Uchida M., Okumura D.: Implicit rule on the elastic function of a swollen polyacrylamide hydrogel. Soft Matter, **17**, 4979–4988 (2021).
https://doi.org/10.1039/D1SM00346A

[34] Chen R., Wang Z., Li S., Du H.: A novel degradation mechanism of the elastic modulus of wet polymer substrates under nanoindentation. Soft Matter, **16**, 5009–5019 (2020).
https://doi.org/10.1039/D0SM00645A

[35] ASTM D790-03: Standard test methods for flexural properties of unreinforced and reinforced plastics and electrical insulating materials (2010).

[36] Ameli A., Datla N. V., Papini M., Spelt J. K.: Hygrothermal properties of highly toughened epoxy adhesives. Journal of Adhesion, **86**, 698–725 (2010).
https://doi.org/10.1080/00218464.2010.482405

[37] Khonakdar H. A., Morshedian J., Wagenknecht U., Jafari S. H.: An investigation of chemical crosslinking effect on properties of high-density polyethylene. Polymer, **15**, 4301–4309 (2003).
https://doi.org/10.1016/S0032-3861(03)00363-X

[38] El Yagoubi J., Lubineau G., Roger F., Verdu J.: A fully coupled diffusion-reaction scheme for moisture sorption-desorption in an anhydride-cured epoxy resin. Polymer, **53**, 5582–5595 (2012).
https://doi.org/10.1016/j.polymer.2012.09.037

[39] Bîrsan M., Pietras D., Sadowski T.: Determination of effective stiffness properties of multilayered composite beams. Continuum Mechanics and Thermodynamics, **33**, 1781–1803 (2021).
https://doi.org/10.1007/s00161-021-01006-2